# Simulation of slug propagation for by-pass pigging in two-phase stratified pipe flow

Hendrix, Maurice; Sanderse, B.; Breugem, Wim-Paul; Henkes, Ruud

**Publication date**
2019

**Document Version**
Final published version

**Published in**
Proc. BHR 19th International Conference on Multiphase Production Technology

# Simulation of slug propagation for by-pass pigging in two-phase stratified pipe flow

*M.H.W. Hendrix*
*Shell Projects & Technology, The Netherlands*
*Delft University of Technology, The Netherlands*

*B. Sanderse*
*Centrum Wiskunde & Informatica (CWI), The Netherlands*

*W.-P. Breugem*
*Delft University of Technology, The Netherlands*

*R.A.W.M. Henkes*
*Shell Projects & Technology, The Netherlands*
*Delft University of Technology, The Netherlands*

**ABSTRACT**

The present paper is focused on the development of an accurate 1D numerical model for pig motion in two-phase flow. The focus will be on the liquid slug that is accumulated in front of the pig, the so-called pig-generated slug. Under the assumption of a stratified flow, we first discuss the academic case of liquid slug accumulation where we neglect the viscosity of the fluids. The size of the liquid slug will then effectively be determined by the speed of the hydrostatic wave which runs ahead of the pig. We also consider the more realistic case which includes the viscosity of the fluid. Finally, we discuss the effect of the presence of a by-pass in the pig on the accumulated liquid slug.

## 1 INTRODUCTION

Several efforts have been made in the past to model the trajectory of a pig, which is propelled by the fluids in a pipeline. These efforts often rely on a 1D cross-sectional description of the fluid, while the pig is modelled as a point mass. The reason for this simplified approach is the high aspect ratio of the problem, which leads to an approach in which only considers variations in the direction of the curvilinear coordinate that runs along the pipeline.

Kohda et al. [1] were among the first to present a numerical method for the motion of a pig in two-phase pipe flow. A separate coordinate system is used for the pig and the fluid. Their simulation results appeared to be in good agreement with experimental data. However, no details were provided on how the two used coordinate systems are coupled. The incorporation of a by-pass in the pig body using a 1D transient single-phase pigging model has been proposed by Nguyen et al. [2], who employed a method of characteristics (MOC) to solve the hyperbolic partial differential equations. Esmaeilzadeh et al. [3] used a MOC approach to model pig motion in a single-phase pipeline, while comparing the modeling results to field data. Nieckele et al. [4] and Hosseinalipour et al. [5] used a finite difference technique to model the motion of a by-pass pig in a single-phase pipeline. Both studies address the necessity of regridding of the numerical grid by using an adaptive mesh as the pig moves through the pipe, but it is not clear whether the approaches are mass conservative. Most of the studies for 1D pig modelling in a pipeline focus on single-phase

flow, only a few consider the presence of a second phase [1, 6, 7, 8]. Among these studies that considered two-phase flow, only pigs without by-pass are considered.

The present paper describes the development of an accurate 1D numerical method to solve the motion of a pig with and without by-pass in a two-phase pipeline. The pig is implemented as a moving border of the numerical grid on which the two-fluid model is solved using a finite-volume method. The two-fluid model that is used is described in detail in [9]. However, in that work only test cases with periodic boundary conditions have been discussed. This is clearly not applicable for monitoring the trajectory of a pig through a pipeline: we will need appropriate boundary conditions at the inlet and outlet of the pipe. We propose the use of characteristic boundary conditions [10, 11]. A similar approach is used to handle the boundary conditions on both sides of the pig. As the pig traverses through the pipe, it is necessary to regrid the finite volumes around the pig, to ensure that the finite-volume sizes do neither get too large nor too small.

The structure of the paper is as follows. The numerical method covering the discretization and boundary treatment is discussed in section 2. The results from the two test cases are discussed in section 3. Section 4 gives conclusions and discusses possibilities for further research.

## 2 NUMERICAL METHOD

The two-fluid model which is used to model the simultaneous transport of a liquid phase and gaseous phase through a pipeline is described in [9, 20]. This two-fluid model assumes a 1D stratified two-phase flow in a pipe. The two-fluid mass and momentum equations read:

$$\frac{\partial}{\partial t}\left(\rho_g A_g\right) + \frac{\partial}{\partial s}\left(\rho_g u_g A_g\right) = 0, \tag{1}$$

$$\frac{\partial}{\partial t}\left(\rho_l A_l\right) + \frac{\partial}{\partial s}\left(\rho_l u_l A_l\right) = 0, \tag{2}$$

$$\frac{\partial}{\partial t}\left(\rho_g u_g A_g\right) + \frac{\partial}{\partial s}\left(\rho_g u_g^2 A_g\right) = -\frac{\partial p}{\partial s} A_g + \frac{\partial HG_g}{\partial s} + \left(-\tau_{gl} P_{gl} - \tau_g P_g\right), \tag{3}$$

$$\frac{\partial}{\partial t}\left(\rho_l A_l\right) + \frac{\partial}{\partial s}\left(\rho_l u_l^2 A_l\right) = -\frac{\partial p}{\partial s} A_l + \frac{\partial HG_l}{\partial s} + \left(\tau_{gl} P_{gl} - \tau_l P_l\right). \tag{4}$$

Here $A_g$ and $A_l$ represent the hold-up of the gas and the liquid phase, respectively. The gas and liquid hold-up make up the total pipe area: $A = A_g + A_l$. The phase velocities for the gas and the liquid are respectively denoted as $u_g$ and $u_l$. The density of the liquid, $\rho_l$, is taken constant, whereas the density of the gas, $\rho_g = \rho_g(p)$, is given by the ideal gas law [9]. Here $p$ is the pressure. $HG_g$ and $HG_l$ denote the hydraulic gradient terms, which are given in [9]. The last two terms of equation (3) and equation (4) represent an expression for the interfacial friction and wall friction. The shear stress of the gas with the pipe wall is denoted as $\tau_g$ and the shear stress of the liquid with the pipe wall is denoted as $\tau_l$. They are expressed by the Fanning friction factor, which is calculated using the Churchill relation, see [9, 12]. The interfacial shear stress $\tau_{gl}$ is calculated according to [13]. $P_g$ and $P_l$ denote the wetted perimeters, whereas $P_{gl}$ represents the length of the interface which separates the gas phase from the liquid phase [9]. The friction terms do not include derivatives of unknown quantities and are identified as the source terms $S_g$ and $S_l$:

 

$$S_g = -\tau_{gl} P_{gl} - \tau_g P_g \,, \tag{6}$$

$$S_l = \tau_{gl} P_{gl} - \tau_l P_l. \tag{7}$$

### 2.1 Spatial discretization

The two-fluid model (equations (1) – (4)) is discretized using the finite-volume method on a staggered grid, see figure 1. The pig is incorporated as a moving border of a finite volume. As a consequence, the discretization of the equations on the finite volumes adjacent to the pig needs to be adjusted. The pig here moves from left to right as a result of a gas and liquid mass influx at the left boundary, which are denoted as $\dot{M}_g$ and $\dot{M}_l$, respectively. The right boundary consists of a pressure outlet condition $p_{out}$.

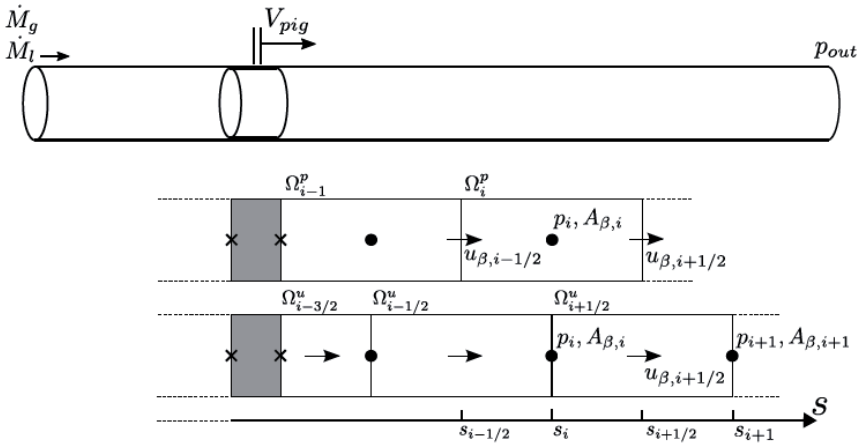


**Figure 1: Staggered grid layout incorporating the presence of a pig.**

The discretization of the mass and momentum equations on finite volumes which lay in the interior of the domain (and thus have no moving boundaries), such as $\Omega^p_i$ and $\Omega^u_{i+1/2}$ as shown in figure 1, is as follows [9]:

$$\frac{d}{dt}\left(\rho_\beta \Omega_\beta\right)_i + \left(\rho_\beta A_\beta\right)_{i+\frac{1}{2}} u_{\beta,i+\frac{1}{2}} - \left(\rho_\beta A_\beta\right)_{i-\frac{1}{2}} u_{\beta,i-\frac{1}{2}} = 0, \tag{8}$$

$$\frac{d}{dt}\left(\rho_\beta u_\beta \Omega_\beta\right)_{i+1/2} + \left(\rho_\beta A_\beta u_\beta^2\right)_{i+1} - \left(\rho_\beta A_\beta u_\beta^2\right)_i = - A_{\beta,i+\frac{1}{2}}\left(p_{i+1} - p_i\right) + \left(HG_{\beta,i+1} - HG_{\beta,i}\right) + S_{\beta,i+\frac{1}{2}}, \tag{9}$$

where

$$\Omega_{\beta,i} = A_{\beta,i} \Delta s_i. \tag{10}$$

Here $\Delta s_i = \left(s_{i+1/2} - s_{i-1/2}\right)$ is the length of the finite volume. We now focus on the discretization of the finite volumes adjacent to the pig, such as $\Omega^p_{i-1}$ and $\Omega^u_{i-3/2}$. For the moment we assume that no by-pass is present in the pig body. As a result, the discretization

of the convective term results in a zero contribution from the left cell face of the finite volume. The spatial discretization of the mass equation for phase $\beta$ (where $\beta = g$ represents gas, and $\beta$ = l represents liquid) on $\Omega_{i-1}^{p}$ then reads:

$$\frac{d}{dt}\left(\rho_\beta \Omega_\beta\right)_{i-1} + \left(\rho_\beta A_\beta\right)_{i-\frac{1}{2}} u_{\beta,i-\frac{1}{2}} = 0. \tag{11}$$

Here $\Omega_{\beta,i-1}$ is a function of time. Similarly, the discretization of the momentum equation on the finite volume $\Omega_{i-3/2}^{u}$ reads:

$$\frac{d}{dt}\left(\rho_\beta u_\beta \Omega_\beta\right)_{i-\frac{3}{2}} + \left(\rho_\beta A_\beta\right)_{i-1} u_{\beta,i-1}^2 = \\ - A_{\beta,i-\frac{3}{2}}\left(p_{i-1} - p_{i-2}\right) + \left(HG_{\beta,i-1} - HG_{\beta,i-2}\right) + S_{\beta,i-\frac{3}{2}}. \tag{12}$$

The discretization of the finite volumes which are located on the left side of the pig are adjusted in a similar way.

## 2.2 Regridding

As the pig traverses through the pipe, the finite volume in front of the pig will reduce in size and the finite volume at the back of the pig will increase in size. We solve our system of equations in conservative form, which means that we solve for the total mass $U_{mass,i} = \rho_{\beta,i}\Omega_i^p$ and for the total momentum $U_{mom,i+1/2} = \left(\rho_\beta u_\beta \Omega_\beta\right)_{i+1/2}$. Since the size of the finite volume is part of the conservative variable $U_{mass,i}$ and $U_{mass,i+1/2}$, the change of the size of the finite volume due to the motion of the pig is naturally captured. The pig motion is solved by applying Newton's second law. The pig position and pig velocity are appended to the vector of unknowns which contains $U_{mass,i}$ and $U_{mom,i+1/2}$ for each finite volume. The resulting system of equations is solved in a monolithic fashion. Since the pig position and pig velocity are part of the solution, there always exists a mapping of $U_i$ to the primitive variables $u_{\beta,i}$, $\rho_{\beta,i}$ and $A_{\beta,i}$.

As a result of the current approach, the finite volume in front of the pig will at some point become too small, whereas the finite volume at the back of the pig will become too large. Therefore, the grid has to be regularly regenerated as the pig traverses through the pipe. We perform the grid regeneration as follows. When the finite-volume cell in front of the pig gets smaller than half the size of a cell as found in the interior, it will be merged with its neighbouring cell. Similarly, if the cell at the back of the pig becomes larger than 1.5 the size of a cell as found in the interior, it will be split up in two cells, see figure 2. The conservative variable $U_i$ will be reconstructed accordingly. The mass $U_{mass,i}^*$ of the volume in front of the pig after regeneration is determined by the sum of the masses of the cells before merging:

$$U_{mass,i+1}^* = U_{mass,i} + U_{mass,i+1}\,. \tag{13}$$

The mass of the cells at the back of the pig is distributed proportionally to the size of the newly created cells:

$$U_{mass,i-1}^* = \frac{\Delta s_{i-1}^* U_{mass,i-1}}{\Delta s_{i-1}}, \tag{14}$$

 

$$U^*_{mass,i} = \frac{\Delta s^*_i U_{mass,i-1}}{\Delta s_{i-1}}. \tag{15}$$

The approach is mass conservative, as $\Delta s^*_{i-1} + \Delta s^*_i = \Delta s_i$. The merging and splitting of momentum cells $U_{mom,i+1/2}$ is performed in the same way.

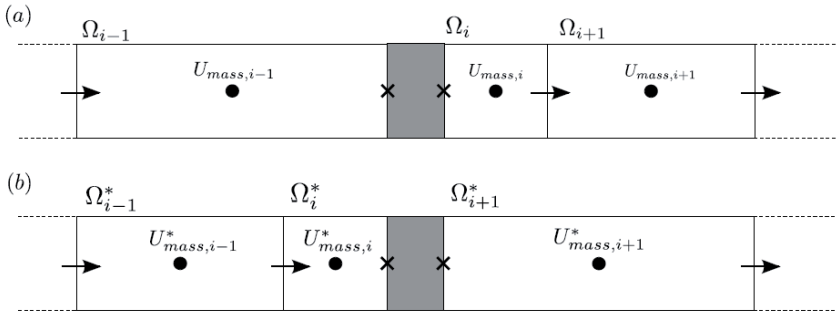


**Figure 2: Grid regeneration. (a) Grid before regeneration. (b) Grid after regeneration.**

We integrate the system of equations in time using the second order BDF2 scheme [9]. Before performing a new time step, the grid is regenerated if necessary. As a result of the regridding procedure as described above, we do not have the solution at the previous time step which exists on the new grid. We therefore change the time integration scheme to Backward Euler for the first time step after regridding for all unknowns, as BDF2 cannot be used since it needs the solution at the previous time step. After having performed the first time step following a regridding procedure, we switch back to the higher order BDF2 scheme.

### 2.3 Boundary conditions

Boundary conditions are implemented using a characteristic boundary treatment [10, 11]. We first write equation (1)-(4) at a boundary point in vector form:

$$\frac{\partial \boldsymbol{U}}{\partial t} + \frac{\partial \boldsymbol{F_0}}{\partial s} + \boldsymbol{D_o}\frac{\partial \boldsymbol{W}}{\partial s} = \boldsymbol{S}. \tag{16}$$

Here $U = [\rho_g A_g, \rho_l A_l, \rho_g u_g A_g, \rho_l u_l A_l]^T$ is the vector containing the conserved variables and $W = [A_l, p, u_g, u_l]^T$ contains the primitive variables. The source terms $S_g$ and $S_l$ are collected in the vector $S = [0,0,S_g,S_l]^T$. We have collected the conservative flux contributions into the second term of equation (16). Here $\boldsymbol{F_0}$ is given by:

$$\boldsymbol{F_0} = \begin{bmatrix} \rho_g u_g A_g \\ \rho_l u_l A_l \\ \rho_g u_g^2 A_g - H G_g \\ \rho_l u_l^2 A_l - H G_l \end{bmatrix}. \tag{17}$$

The non-conservative flux contributions are collected into the third term of equation (16). Here $D_0$ is given by:

$$\boldsymbol{D_0} = \begin{bmatrix} 0 & 0 & 0 & 0 \\ 0 & 0 & 0 & 0 \\ 0 & A_g & 0 & 0 \\ 0 & A_l & 0 & 0 \end{bmatrix}. \tag{18}$$

We now put equation (16) in quasi-linear form by defining Jacobian matrix $\boldsymbol{A_0} = \frac{\partial \boldsymbol{U}}{\partial \boldsymbol{W}}$ and $\boldsymbol{J_0} = \frac{\partial \boldsymbol{F_0}}{\partial \boldsymbol{W}}$:

$$\boldsymbol{A_0}\frac{\partial \boldsymbol{W}}{\partial t} + \boldsymbol{J_0}\frac{\partial \boldsymbol{W}}{\partial s} + \boldsymbol{D_0}\frac{\partial \boldsymbol{W}}{\partial s} = \boldsymbol{A_0}\frac{d\boldsymbol{W}}{dt} + \boldsymbol{B_0}\frac{\partial \boldsymbol{W}}{\partial s} = \boldsymbol{S}. \tag{19}$$

Here $\boldsymbol{B_0} = \boldsymbol{J_0} + \boldsymbol{D_0}$, and is given as follows:

$$\boldsymbol{B_0} = \begin{bmatrix} -u_g\rho_g & A_g u_g \frac{\partial \rho_g}{\partial p} & A_g\rho_g & 0 \\ u_l\rho_l & 0 & 0 & A_l\rho_l \\ -u_g^2\rho_g - \frac{\partial HG_g}{\partial A_l} & A_g\left(u_g^2\frac{\partial \rho_g}{\partial p} + 1\right) - \frac{\partial HG_g}{\partial p} & 2A_g u_g\rho_g & 0 \\ -u_l^2\rho_l - \frac{\partial HG_l}{\partial A_l} & A_l & 0 & 2A_l u_l\rho_l \end{bmatrix}. \tag{20}$$

We now multiply equation (19) with $\boldsymbol{A_0^{-1}}$ to obtain:

$$\frac{\partial \boldsymbol{W}}{\partial t} + \boldsymbol{Q}\frac{\partial \boldsymbol{W}}{\partial s} = \boldsymbol{A_0^{-1}}\mathbf{S}. \tag{21}$$

Here $\boldsymbol{Q} = \boldsymbol{A_0^{-1}}\boldsymbol{B_0}$ is given by:

$$\boldsymbol{Q} = \begin{bmatrix} u_l & 0 & 0 & A_l \\ -\frac{\rho_g(u_g - u_l)}{A_g\frac{\partial \rho_g}{\partial p}} & u_g & \frac{\rho_g}{\frac{\partial \rho_g}{\partial p}} & \frac{A_l\rho_g}{A_g\frac{\partial \rho_g}{\partial p}} \\ -\frac{\frac{\partial HG_g}{\partial A_l}}{A_g\rho_g} & A_g - \frac{\frac{\partial HG_g}{\partial p}}{A_g\rho_g} & u_g & 0 \\ -\frac{\frac{\partial HG_l}{\partial A_l}}{A_l\rho_l} & \frac{1}{\rho_l} & 0 & u_l \end{bmatrix}. \tag{22}$$

To derive characteristic equations, from which time dependent equations for the boundary points can be obtained, we determine the eigendecomposition of $\boldsymbol{Q} = \boldsymbol{R\Lambda R^{-1}}$. Here $\boldsymbol{\Lambda}$ contains the eigenvalues $[\lambda_1, \lambda_2, \lambda_3, \lambda_4]^T$ on the diagonal and $\boldsymbol{R}$ contains the right eigenvectors of $\boldsymbol{Q}$:

$$\frac{\partial \boldsymbol{W}}{\partial t} + \boldsymbol{R\Lambda R}^{-1}\frac{\partial \boldsymbol{W}}{\partial s} = \boldsymbol{A_0^{-1}}\mathbf{S}. \tag{23}$$

The eigenvalues and eigenvectors can be computed analytically with the help of a computer algebra system. However, the expressions which are obtained are long, so we will not reproduce them here. Now we define the vector $\boldsymbol{L} = \boldsymbol{\Lambda R}^{-1} \frac{\partial \boldsymbol{W}}{\partial s}$ and rewrite equation (23) as follows:

$$\frac{\partial \boldsymbol{W}}{\partial t} + \boldsymbol{R}\mathbf{L} = \boldsymbol{A}_\mathbf{0}^{-1}\mathbf{S}. \tag{24}$$

Here the components of $\boldsymbol{L} = [L_1, L_2, L_3, L_4]^T$ are associated to the eigenvalues $[\lambda_1, \lambda_2, \lambda_3, \lambda_4]^T$. The four eigenvalues of the compressible two-fluid model, assuming subsonic flow, contain one negative and one positive eigenvalue close to the speed of sound, say $\lambda_1$ and $\lambda_4$, respectively. The magnitude of the other two eigenvalues, $\lambda_2$ and $\lambda_3$, are in the order of the phase velocities and their sign depends on the local flow conditions [9, 14]. We thus consider the following three possibilities: $\lambda_2$ and $\lambda_3$ are both positive, $\lambda_2$ and $\lambda_3$ are both negative, and $\lambda_2$ is negative while $\lambda_3$ is positive. We use the sign of the eigenvalues to determine the number of incoming and outgoing waves at the boundary. By solving equation (24) we can then formulate time dependent equations for the solution at the boundary points. For example, we consider the right boundary point, which corresponds to the outlet of the domain for the cases considered in this work. Figure 3 shows the grid layout near the right boundary point.

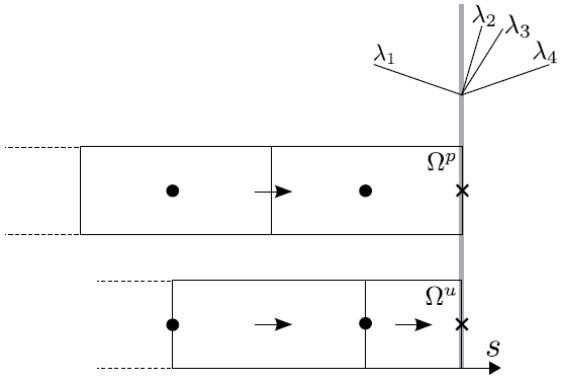


**Figure 3: Schematic of the grid layout near the right boundary point.**

The eigenvalues can be calculated at the boundary point as function of the current solution at the boundary point. A possible outcome could be that $\lambda_2$ and $\lambda_3$ are both positive, which would imply that we have three positive eigenvalues and one negative eigenvalue (since $\lambda_1$ and $\lambda_4$ are negative and positive respectively). Since we consider the right boundary, three positive eigenvalues correspond to three outgoing waves. This means that the components $L_2$, $L_3$ and $L_4$ of vector $\boldsymbol{L}$ which feature $\frac{\partial \boldsymbol{W}}{\partial s}$ can be calculated by using finite differences which are evaluated using the interior of the domain. $L_1$ should not be calculated in this case, since it corresponds to an incoming wave, and no information is available in the interior of the domain. Instead information should be given by supplying an appropriate boundary condition by providing an expression for one of the entries in the vector $\frac{\partial \boldsymbol{W}}{\partial t}$. A typical boundary condition for an outlet used in this work is an outlet

condition for the pressure. A constant outlet pressure corresponds to $\frac{\partial \boldsymbol{p}}{\partial t} = 0$. Equation (24) can now be completely solved since we have 4 unknowns ($L_1$ and the remaining three unknown entries of vector $\frac{\partial \boldsymbol{W}}{\partial t}$) and 4 equations. The result is an expression for the full vector $\frac{\partial \boldsymbol{W}}{\partial t}$ at the boundary point, which can be integrated together with the interior using the BDF2 scheme. For the left boundary of the domain and the pig boundaries we employ the same technique. For the pig boundaries this results in a boundary condition for the fluid velocity from which the liquid hold-up and pressure can be calculated. For some boundary conditions it may be more convenient to express the boundary equations in terms of conserved variables $\boldsymbol{U}$ instead of primitive variables $\boldsymbol{W}$. For example, at the inlet of the domain one would rather supply boundary conditions in terms of the gas and liquid mass inflow than in terms of gas and liquid velocity. To derive boundary equations in terms of $\boldsymbol{U}$, equation (24) is multiplied by the Jacobian $\boldsymbol{A_0}$.

## 3 TEST CASES

In this section we discuss two test cases which were performed using the method described in the previous section. In these test cases we focus on the liquid slug that is accumulated in front of the pig, see figure 4. In describing the liquid slug we make use of the definition of the liquid hold-up fraction:

$$\alpha = \frac{A_l}{A}. \tag{25}$$

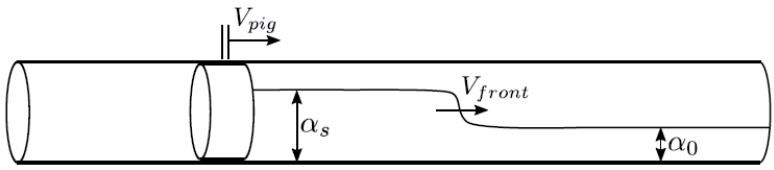


**Figure 4: Schematic of liquid slug accumulation in front of a moving pig.**

Due to the movement of the pig an increased liquid hold-up fraction $\alpha_s$ exists in this pig-generated slug when compared to the hold-up fraction further downstream, which we denote as $\alpha_0$. We also define the velocity of the transient that travels ahead of the pig, $V_{front}$. This front separates two regions: the region downstream of the front, where the flow is still unaffected by the pig motion, and the region upstream of the front where the flow is affected as a result of the pig motion. We first discuss a test case which considers a pig without by-pass. We then move to a test case for pigs with by-pass.

### 3.1 Pig-generated slug for pigs without by-pass

As a first step in understanding the liquid slug which is propelled by a pig in two-phase stratified pipe flow, we assume inviscid flow and a preset pig velocity. In addition, we neglect the pressure gradient $\frac{\partial p}{\partial s}$, which means that we only consider pressure variations due to the hydraulic gradient term. We can then simplify the liquid mass equation (2) and the liquid momentum equation (4). When applying a mass and momentum balance over the liquid front in a reference frame that moves with the liquid front we can then write the following steady-state balance:

 

$$\left(V_{pig} - V_{front}\right)\alpha_s A = \left(-V_{front}\right)\alpha_0 A, \tag{26}$$

$$\left(V_{pig} - V_{front}\right)^2 \alpha_s A \; - HG_{l,\alpha=\alpha_s} = \left(-V_{front}\right)^2 \alpha_0 A - HG_{l,\alpha=\alpha_0}. \tag{27}$$

Here $HG_{l,\alpha=\alpha_s}$ is the hydraulic gradient term evaluated in the slug region in front of the pig, whereas $HG_{l,\alpha=\alpha_0}$ is the hydraulic gradient term evaluated downstream of the liquid front. Inspecting equation (26) and (27) we identify two unknowns which characterize the pig-generated slug: $\alpha_s$ and $V_{front}$. We solve for $\alpha_s$ and $V_{front}$ and compare the result with numerical simulations of the full two-fluid model (equation (1)-(4)), see figure 5.

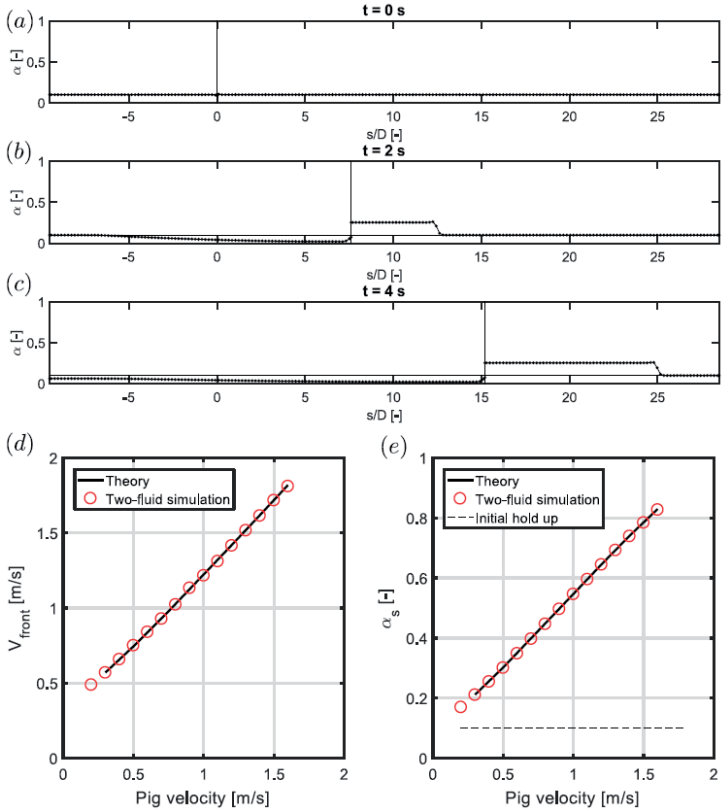


**Figure 5: Pig-generated slug for inviscid flow. (a) Initial condition at $t$ = 0 s. The spatial coordinate $s$ is normalized by the pipe diameter $D$. (b) Solution a $t$ = 2 s. (c) Solution at $t$ = 4 s. (d) $V_{front}$ as function of the pig velocity. (e) $\alpha_s$ as function of the pig velocity.**

The simulations were carried out by considering a pipeline with initial hold-up of $\alpha_0$ = 0.1, with the fluid being at rest. At time $t$ = 0 s, a pig is inserted at $s$ = 0 m, which is visible in figure 5a as a vertical black line. The pig is given a constant preset velocity $V_{pig} = 0.4$ m/s, and as a result liquid is accumulated in front of the pig, see figure 5b/c. We use the properties of water for the liquid phase, whereas we use the properties of air for the gas phase. The time step is taken as $dt = 0.0025$ s, whereas the number of volumes is 200.

The domain length is 4 m, which results in a mesh size of $ds = 0.02$ m. The other simulation parameters are summarized in table 1.

**Table 1: Simulation parameters.**

| Parameter | Value |
|---|---|
| Liquid density $\rho_l$ | 998 kg/m$^3$ |
| Gas speed of sound $c_g$ | 289 m/s |
| Liquid viscosity $\mu_l$ | 0.001 kg/(ms) |
| Gas viscosity $\mu_g$ | 0.0000181 kg/(ms) |
| Pipe diameter $D$ | 0.105 m |
| Pipe wall roughness $\epsilon$ | 0.000005 m |
| Acceleration of gravity $g$ | 9.8 m/s$^2$ |
| Outlet pressure $p_{out}$ | 100000 Pa |

From the simulation results $\alpha_s$ and $V_{front}$ can be extracted, see figure 5d/e in which the results for various pig velocities are summarized. A good agreement is found when comparing the simulation result to the theoretical solution for $\alpha_s$ and $V_{front}$, which is obtained from solving equations (26) and (27).

As a next step we consider the same test case, but we include the viscosity of the fluid. The viscosity of the liquid phase will generate an increasing amount of friction with the pipe wall. As a result, the liquid hold-up $\alpha_s$ in the pig-generated slug keeps increasing until it hits the top of the pipe, see figure 6. For this simulation $V_{pig} = 1.0$ m/s. The time step is taken as $dt = 0.02$ s, whereas the number of volumes is 200. The domain length is 120 m, which results in a mesh size of $ds = 0.6$ m. As a consequence of the liquid that hits the top of the pipe for pigs without by-pass, an initial full-bore liquid slug is formed, which finally can result in a large liquid surge that must be managed by the receiving facilities [19]. The use of a by-pass pig can help to smooth out the liquid surge [19]. This will be the topic of the next section.

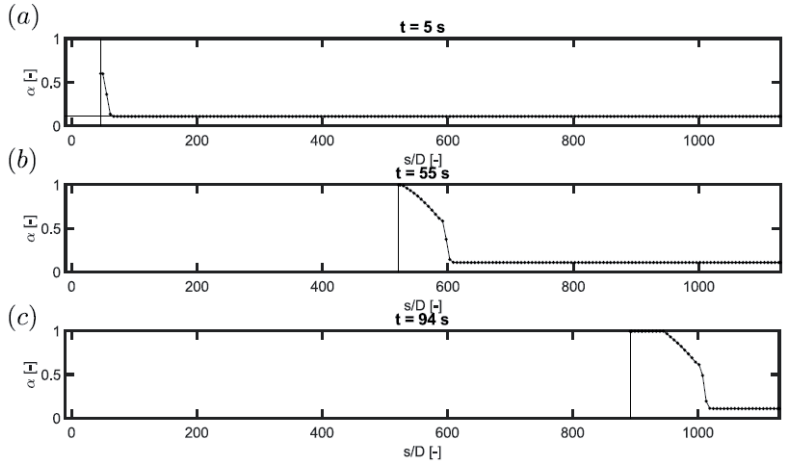


**Figure 6: Pig-generated slug for viscous flow. (a) Solution at *t* = 5 s. (b) Solution at t = 55 *s*. (c) Solution at *t* = 94 s.**

 

### 3.2 Pig-generated slug for pigs with by-pass

The presence of a by-pass in the pig body has two effects on the pig-generated slug. First of all, a by-pass pig will a have lower travel velocity compared to a conventional pig. The steady-state velocity of a by-pass pig in a horizontal pipe can be expressed as follows [15, 16]:

$$V_{pig} = V_{mix} - \frac{d^2}{D^2}\frac{\rho_{bp}}{\rho_{up}}\sqrt{\frac{F_{fric}}{K\frac{1}{2}\rho_{bp}A}}. \tag{28}$$

Here $V_{mix}$ is the upstream mixture velocity, $d$ is the diameter of the by-pass hole, $\rho_{bp}$ is the density of the fluid in the by-pass (which is taken as the downstream gas density), $\rho_{up}$ is the upstream density of the gas, $F_{fric}$ is friction of the pig with the inner pipe wall, and $K$ is the pressure loss coefficient of the by-pass pig. We use the Idelchik relation to calculate $K$, in which we assume single-phase gas flow around the by-pass pig [16-18]. The pig length for calculating $K$ is taken equal to two times the pipe diameter $D$. Furthermore, we take a value of $F_{fric} = 10$ N. When the by-pass area fraction $\frac{d^2}{D^2}$ goes to zero, one retrieves a pig velocity equal to the upstream mixture velocity. As a result of the lower pig velocity due to the by-pass, the liquid in front of the pig will also adopt a lower velocity.

A second effect of the presence of a by-pass is that the gas that by-passes will result in a liquid hold-up $\alpha_s$ in front of the pig, which is not equal to one, i.e. the liquid will not reach the top of the pipe. Instead, $\alpha_s$ will reach an equilibrium hold-up; see the results in figure 7 for different by-pass ratios. As an initial condition the hold-up fraction has again been settled at 0.1, which was achieved by setting $\dot{M}_l = 0.051$ kg/s and $\dot{M}_g = 0.010$ kg/s at the inlet. We carried out a simulation for a pig with a by-pass area fraction of 0.02, which results in $V_{pig} = 0.3427$ m/s (equation (28)). The time step is taken as $dt = 0.64$ s, whereas the number of volumes is 200. The domain length is 960 m, which results in a mesh size of $ds = 4.8$ m. All other simulation parameters are summarized in table 1. To avoid additional transients due to initial acceleration of the pig, we directly set the pig velocity equal to the steady-state pig velocity, as given by equation (28). The equilibrium hold-up $\alpha_s$ is extracted when the hold-up in front of the pig has settled to a steady-state value, see figure 7c.

We now proceed to estimate $\alpha_s$ by a simplified model. We therefore again consider the region just downstream of the pig, where $\alpha = \alpha_s$. As a first step we aim to have an expression for the liquid and gas mass flow in this region, denoted $\dot{M}_{l,\alpha=\alpha_s}$ and $\dot{M}_{g,\alpha=\alpha_s}$. As the liquid velocity has adopted the pig velocity, the $\dot{M}_{l,\alpha=\alpha_s}$ can be calculated as follows:

$$\dot{M}_{l,\alpha=\alpha_s} = \rho_l V_{pig}\alpha_s A. \tag{29}$$

The gas mass flow at this location is determined by the amount of gas that goes through the by-pass pig. It can be calculated by applying a mass balance:

$$\dot{M}_{g,\alpha=\alpha_s} = \rho_{up}(V_{mix} - V_{pig})A. \tag{30}$$

We next use the steady-state limit of the momentum equations (3) and (4) where we neglect spatial derivatives (except for the pressure gradient), to derive the following point model:

$$\tau_{gl} P_{gl} \left( \frac{1}{1-\alpha_s} + \frac{1}{\alpha_s} \right) + \frac{\tau_g P_g}{1-\alpha_s} - \frac{\tau_l P_l}{\alpha_s} = 0. \tag{31}$$

Here the shear stresses are a function of $\alpha_s$ as well as the gas and liquid mass flow, which are given by equation (29) and (30). As $\alpha_s$ is the only unknown in equation (31), it can be solved, see figure 7d. This simplified approach shows good agreement with the numerical simulations, which thus gives insight in characterizing the liquid slug which is propelled by a by-pass pig under the assumption of stratified flow conditions.

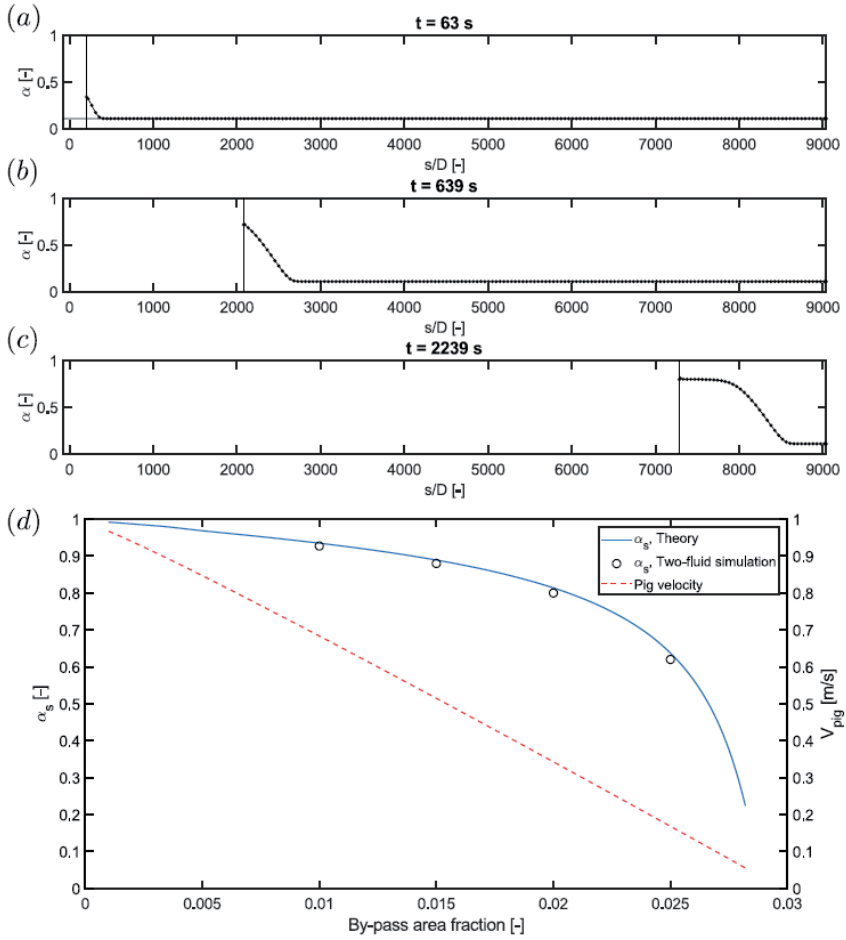


**Figure 7: Pig-generated slug for a by-pass pig. (a) Solution condition at *t* = 63 s. The by-pass area fraction is equal to 0.02. (b) Solution at *t* = 639 s. (c) Solution at *t* = 2239 s. (d) $\alpha_s$ and pig velocity as a function of the by-pass area fraction.**

## 4 CONCLUSIONS

In this paper we have discussed the numerical implementation of the pig motion in stratified two-phase pipe flow using a mass conserving two-fluid model. The pig has been implemented as a moving border of a finite volume. A new mass- and momentum-conserving regridding strategy has been proposed and a new implementation of the boundary condition treatment has been realized. Test cases were used to characterize the liquid slug accumulation in front of the pig for both inviscid and viscous flow. The effect of a by-pass in the pig body on the liquid slug has been quantified. Good agreement between the simplified approach and the 1D transient simulations was found.

The current study has been carried out assuming stratified flow. This assumption may not always hold, especially not for the flow just in front of the pig, which may depend on the details of the shape of the pig and of the by-pass holes. A 1D pipe flow model will in general not be able to predict the complex 3D flow close to the by-pass pig. Therefore, it is recommended to carry out two-phase CFD simulations to help developing reliable two-phase correlations which characterize the flow just in front of the by-pass pig. The correlations will serve as input to the 1D model, such as the model presented in this study. The pig velocity in this study was given the preset steady-state velocity from the start of the simulation. A next step is to test if the assumptions of the simplified model will still hold when startup transients of the pig and the surrounding fluid are included in the full 1D simulation.

## REFERENCES


1. Kohda, K., Suzukawa, Y., and Furukawa, "New method for analyzing transient flow after pigging scores well", Oil and Gas Journal 86, pp. 40-47, 1988.
2. Nguyen, T.T., Kim, S.B., Yoo, H.R., and Rho, Y.W., "Modelling and simulation for a pig with bypass flow control in a natural gas pipelines", KSME Int. Journal 15, pp. 1302-1310, 2001.
3. Esmaeilzadeh, F., Mowla, D., and Asemani, M., "Mathematical modeling and simulation of pigging operation in gas and liquid pipelines", J. of Petroleum Science and Engineering 69, pp. 100-106, 2009.
4. Nieckele, A.O., Braga, A.M.B., and Azevedo, L.F.A., "Transient pig motion through gas and liquid pipelines", J. of Energy Resources Technology, Trans. ASME, 123, pp. 260-268, 2001.
5. Hosseinalipour, S.M., Zariff Khalili, A., Salimi, A., "Numerical simulation of pig motion through gas pipelines", Proc. 16th Australasian Fluid Mechanics Conf., pp. 971-975, 2007.
6. Jamshidi, B., and Sarkari, M., "Simulation of pigging dynamics in gas-liquid two-phase flow pipelines", Journal of Natural Gas Science and Engineering 32, pp. 407–414, 2016.
7. Minami K., and Shoham O., "Pigging dynamics in two-phase flow pipelines: Experiment and Modeling", SPE Production and Facilities 10, pp. 225–231, 1995.
8. Xu X., and Gong J., "Pigging simulation for horizontal gas-condensate pipelines with low liquid loading", Journal of Petroleum Science and Engineering 48, pp. 272–280, 2005.
9. Sanderse, B., Smith, I.E., and Hendrix, M.H.W., "Analysis of time integration methods for the compressible two-fluid model for pipe flow simulations", Int. J. Multiphase Flow 95, pp. 155-174, 2017.

10. Olsen, R., “Time Dependent Boundary Conditions for Multiphase Flow”, PhD Thesis. NTNU, 2004.
11. Thompson, K.W., “Time dependent boundary conditions for hyperbolic systems” Journal of Computational Physics 68, pp. 1–24, 1987.
12. Churchill, S.W., “Friction-factor equation spans all fluid flow regimes”, Chemical engineering 84, pp. 91–92, 1977.
13. Liao J., Mei R., and Klausner J.F., “A study on the numerical stability of the two-fluid model near ill-posedness”, International Journal of Multiphase Flow 34, pp. 1067–1087, 2008.
14. Figueiredo, A.B., Baptista R.M., Freitas Rachid, F.B., and Bodstein, G.C.R., “Numerical simulation of stratified-pattern two-phase flow in gas pipelines using a two-fluid model”, International Journal of Multiphase Flow 88, pp. 30–49, 2017.
15. Hendrix, M.H.W., IJsseldijk, H.P., Breugem, W.-P., and Henkes, R.A.W.M., “Experiments and modelling of by-pass pigging under low pressure conditions”, Journal of Process Control 71, pp. 1-13, 2018.
16. Singh, A. and Henkes, R.A.W.M., “CFD modeling of the flow around a by-pass pig”, Proc. 8th North American Conference on Multiphase Technology, pp. 229-243, 2012.
17. Hendrix, M.H.W., Liang, X., Breugem, W.-P., and Henkes, R.A.W.M., “Characterization of the pressure loss coefficient using a building block approach with application to by-pass pigs”, Journal of Petroleum Science and Engineering, 150: 13 - 21, 2017.
18. Idelchik, I.E., “Handbook of Hydraulic Resistance”, 2nd edition, Hemisphere Publishing Corporation, 1987.
19. Entaban, A., Ismail, A., Jambari, M., Ting, P., Amin, K.M., Ping, C.C., Zou, S., and Van Spronsen, G., “By-pass pigging - a ‘simple’ technology with significant business impact”, International Petroleum Technology Conference, pp. 1-6, 2013.
20. Sanderse, B., and Veldman, A.E.P., “Constraint-consistent Runge-Kutta methods for one-dimensional incompressible multiphase flow”, Journal of Computational Physics, In Press, doi:10.1016/j.jcp.2019.02.001, 2019.